View metadata, citation and similar papers at core.ac.uk

brought to you by CORE

provided by RERO DOC Digital Library

Appl. Phys. B 91, 257–264 (2008)

DOI: 10.1007/s00340-008-2973-y

Applied Physics B

Lasers and Optics

OpenAccess

P. KREUTER[1]
B. WITZIGMANN[1]
D.J.H.C. MAAS[2]
Y. BARBARIN[2]
T. SÜDMEYER[2]
U. KELLER[2,✉]

On the design of electrically pumped vertical-external-cavity surface-emitting lasers

[1] Integrated Systems Laboratory, Department of Information Technology and Electrical Engineering, ETH Zurich, Gloriastr. 35, 8092 Zurich, Switzerland

[2] Institute of Quantum Electronics, Physics Department, ETH Zurich, Wolfgang-Pauli-Str. 16, 8093 Zurich, Switzerland

Received: 6 February 2008
Published online: 12 March 2008 • **© The Author(s) 2008**

ABSTRACT Vertical-external-cavity surface-emitting lasers (VECSELs) yield an excellent beam quality in conjunction with a scalable output power. This paper presents a detailed numerical analysis of electrically pumped VECSEL (EP-VECSEL) structures. Electrical pumping is a key element for compact laser devices. We consider the optical loss, current confinement, and device resistance. The main focus of our investigation is on the achievement of an adequate radial carrier distribution for fundamental transverse mode operation. It will be shown that a trade off between the conflicting optical and electrical optimization has to be found and we derive an optimized design resulting in guidelines for the design of EP-VECSELs which are compatible with passive mode locking.

PACS 42.55.Px; 42.60.By; 85.30.De

1 Introduction

Vertical-external-cavity surface-emitting lasers (VECSELs) [1] are of high scientific and industrial interest due to their large fundamental transverse mode output power, scaling with the device radius, the near diffraction limited output beam, and the suitability for intracavity frequency conversion [2] and passive mode locking [3, 4]. Passive mode locking of an optically pumped VECSEL has been demonstrated with a semiconductor saturable absorber mirror (SESAM) [5] in a folded external cavity. After the first passively mode locked VECSEL was demonstrated in the year 2000 [6], the milestone of nearly 1 W average output power was achieved in 2002 with improved thermal management [7]. The pulses in the early experiments were often strongly chirped, but mode-locking dynamics in VECSELs revealed that a soliton-like pulse-shaping mechanism in the positive-dispersion regime can help to generate short pulses with low chirp. With the aid of intracavity dispersion control, it then became possible to obtain nearly transform limited picosecond pulses with record high output powers of 2.1 W at 4 GHz [4] and 1.4 W at 10 GHz [8]. The pulse width could be significantly shortened to the sub-500-fs regime using faster SESAMs based on the ac Stark effect [9]. The vertical integration of the absorber into one monolithic structure with the gain quantum wells (QWs) is an important step towards higher pulse repetition rates with decreased cavity size and wafer-scale integration. This has been achieved for the first time and is referred to as the mode-locked integrated-external-cavity surface-emitting laser (MIXSEL) [10]. So far, all these devices have been optically pumped, which involves a more complex optical setup. Thus, an important step towards wafer-scale fabrication of compact ultrafast VECSELs is the design of electrically pumped VECSEL (EP-VECSEL) structures. This is challenging because of optical losses and Joule heating in the doped layers. Nevertheless, continuous-wave (cw) EP-VECSELs have been demonstrated [11, 12] and output powers of up to 900 mW have been obtained with a 150-μm device diameter in multimode operation [13]. Also, mode locking with down to 15-ps FWHM pulse width [14] and a wafer-scale EP-VECSEL with a micromirror and 10-mW cw output power have been reported [15]. So far, the average output power of passively mode locked EP-VECSELs has been limited to 40 mW [16] even though nearly 1 W of average power has been demonstrated at cw.

Although EP-VECSELs have already been demonstrated, there is not yet a systematic methodology of how to design EP-VECSELs. The rather low average power of ultrafast EP-VECSELs demonstrated so far suggests that the EP-VECSEL needs to be designed and optimized also for mode-locking operation and not only for maximum cw output power. Many different design guidelines can be found in [17] for vertical-cavity surface-emitting lasers (VCSELs), which do not exhibit an external cavity. For these types of lasers, the use of technology computer aided design (TCAD) for the analysis and design is an established approach [18].

In this paper, we discuss several designs of EP-VECSELs which are compatible with passive mode locking using microscopic simulation. The paper is organized as follows. In Sect. 2 we comment briefly on the numerical approaches we use for carrier transport and optical loss simulation. The successive derivation of the device design and the optimization of the key components is accomplished in Sect. 3. Eventually, Sect. 4 is devoted to concluding the paper and to outline future work.

✉ Fax: +41-44-633-10-59, E-mail: keller@phys.ethz.ch

2 Numerical approach

For the description of bulk carrier transport in the investigated EP-VECSEL structures a standard drift–diffusion model, derived from the Boltzmann transport equation by the method of moments, is applied [19]. Thus, the charge carrier flux equations relating the electron and hole current densities j_n and j_p to the electron and hole densities n and p and the electrostatic potential Ψ read

$$\boldsymbol{j}_n = -q\left(\mu_n n \nabla\Psi - D_n \nabla n + \frac{3}{2} D_n n \nabla \ln m_{\mathrm{e}}\right) , \quad (1)$$

$$\boldsymbol{j}_p = -q\left(\mu_p p \nabla\Psi + D_p \nabla p - \frac{3}{2} D_p p \nabla \ln m_{\mathrm{h}}\right) , \quad (2)$$

with $\mu_{n,p}$ being the carrier mobilities, $D_{n,p}$ the diffusion coefficients, and q the elementary charge. The third term in (1) and (2) takes spatially inhomogeneous effective masses $m_{\mathrm{e,h}}$ into account, which occur in regions with graded mole fractions [20]. The above equations are completed by the Poisson equation

$$\nabla(\varepsilon\nabla\Psi) = -q\left(p - n + N_{\mathrm{D}}^{+} - N_{\mathrm{A}}^{-}\right) , \quad (3)$$

with the permittivity of the semiconductor ε, the ionized donor and acceptor concentrations N_{D}^{+} and N_{A}^{-}, and the continuity equations

$$\nabla \cdot \boldsymbol{j}_n = q\left(R + \delta_t n\right) , \quad (4)$$

$$-\nabla \cdot \boldsymbol{j}_p = q\left(R + \delta_t p\right) , \quad (5)$$

with the total recombination rate R (Shockley–Read–Hall, Auger, and spontaneous recombination). In addition, a thermionic emission model is used to address abrupt heterointerfaces [21].

In a VECSEL the transverse optical mode profile is governed by the external mirror ensuring fundamental (TEM_{00}) transverse mode operation. Since the influence of the refractive-index distribution in the cavity on the transverse mode is much smaller than that of the external mirror, we can approximate the fundamental transverse mode by a paraxial Gaussian beam and decompose the electrical field into a longitudinal profile times the TEM_{00} mode [22]. The calculation of the longitudinal mode profile is carried out using a one-dimensional transfer-matrix method and optical losses due to free-carrier absorption (FCA) are taken into account via a complex propagation constant for the calculation of the mirror reflectivities. The investigation is limited to operation below and at threshold, with the aim to optimize carrier injection for maximum fundamental transverse mode gain. Hence, self heating of the device is not considered.

3 Device design

The design of an electrically pumped VECSEL is quite demanding, since it has to fulfill several partially competing device constraints. Figure 1 shows the sketch of the semiconductor part of an EP-VECSEL identifying the constitutive device components. The external cavity is indicated by the curved mirror on top. Note that the linear external cavity shown here is just an example and one might apply any other external-cavity design (e.g. Z- and V-shaped external cavities [4]). In the following, we will focus on the semiconductor part of the VECSEL. A very important issue for fundamental mode operation is the confinement of the charge carriers and thus the inversion region to the mode area in the center of the device. In optically pumped VECSELs the extracted output power can easily be enhanced by increasing the pump spot size and the spatial mode due to the one-dimensional heat flow. For an EP-VECSEL this means that carrier confinement should also be scalable, to allow for an increased homogeneous inversion area, which also results in constraints on the contact design. However, the design of the top contact is constrained by the necessity to couple the light from the semiconductor part of the structure into the external cavity. Another obstacle in EP-VECSEL design is the high resistance of the distributed Bragg reflector (DBR) mirror, which has to be minimized to avoid excessive heating of the device. This can be circumvented by high doping levels in the DBR, which, however, are prohibitive in an EP-VECSEL due to the increased optical loss caused by FCA. Given the rather small round-trip gain achieved in vertical-emitting lasers, optical losses are critical in the device design. Furthermore, the device should yield a broad spectral range that is essential for achieving ultra-short pulses when mode locked by insertion of a saturable absorber. The growth and processing of the structure satisfying the above requirements should be kept as simple as possible to, eventually, allow for low-cost fabrication of the device.

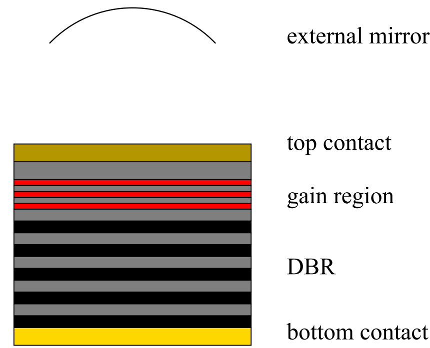

FIGURE 1 Sketch of an EP-VECSEL design (not to scale)

In the following, we present the derivation of a recommended EP-VECSEL design starting with a device as shown in Fig. 1 and taking into account the primary design considerations outlined above. Even if the optimization of each parameter of the device is not independent of the others, we try to focus on distinct device components in each of the sections below for the sake of clarity. The implications of design variations in a certain component on the remainder of the structure are mentioned explicitly.

3.1 *n- vs. p-doped DBR and contact geometry*

In vertical-emitting laser devices like the VECSEL the gain per round trip is rather small due to the thin active region, resulting in the need for highly reflective distributed Bragg reflectors as cavity end mirrors. In the case of the VECSEL, one of the two end mirrors is replaced by a curved external mirror which is used to define the transverse mode profile. The device performance of EP-VECSELs

is severely limited by the interface potential barriers within the DBR mirror, resulting in a high resistance. Driving the current through the mirrors thus yields a high power loss and Joule heating of the device, which in turn degrade its overall characteristics. Hence, a sophisticated design is necessary to facilitate electrical pumping, especially through p-doped DBRs where the low hole mobilities otherwise yield a prohibitively high device resistance. Several solutions like heavy doping, various types of mole fraction grading, and δ-doping of the interfaces have been developed to circumvent this problem in VCSELs [17, 23, 24]. Since the electron and hole mobilities as well as the conduction-band and valence-band offsets in an AlGaAs-based DBR differ significantly, different measures have to be taken for n- and p-DBRs in order to achieve acceptable device resistances. Investigations of p-DBR structures by simulation show that the interfaces between the quarter-wavelength layers have to be implemented with a mole fraction grading to facilitate laser operation (cf. Fig. 2). Another possibility to decrease the DBR resistance is the use of ternary AlGaAs layers instead of AlAs/GaAs interfaces, which reduces the band offset. However, the reflectivity of the mirror is also lowered and the number of layer pairs has to be increased in order to meet a fixed minimum reflectivity. Doping is another critical issue in DBRs since, on the one hand, it introduces additional FCA losses to the optical field but, on the other hand, it is essential for electrical pumping. Hence, moderate doping has to be applied in order to obtain a good trade off between low loss and low resistance. A reasonable p-DBR design features a 20-nm grading layer with a doping concentration of approximately $N_A = 2 \times 10^{18}$ cm^{-3} (see Fig. 2) and an n-DBR could be implemented as an $Al_{0.9}Ga_{0.1}As/Al_{0.2}Ga_{0.8}As$ mirror without grading or a graded AlAs/GaAs mirror. The applied doping level equals that of the p-DBR. However, the FCA losses are approximately a factor of two smaller [25] in the n-doped mirror and it also exhibits a smaller resistance. Furthermore, the ungraded n-mirror allows for a simple growth. Thus, we could conclude that an n-doped rather than a p-doped DBR in Fig. 1 is preferred. However, the additional requirements for uniform current injection will determine the final doping selection.

The laser light emitted in the active region has to be coupled out into the external cavity, which renders a central top contact for current confinement impossible. Thus, a more sophisticated design of the top contact is necessary. A common solution to this problem in VCSELs is a ring contact on top of the device which is sometimes implemented as an intracavity ring contact to avoid pumping through the top mirror. In an EP-VECSEL there is either no top DBR or only a low-reflection, low-resistance mirror for gain enhancement [13]. An anti-reflection (AR) coating on top of the semiconductor part of the device should be applied to reduce structural dispersion and bandwidth filtering of the device. This is particularly important if the VECSEL is mode locked. Pumping through the AR coating can also be circumvented with a ring contact (see Fig. 10).

Using a design with a top ring contact and an unstructured bottom contact without any additional measures for current confinement, we obtain a design similar to the structure depicted in Fig. 3 with the difference that the bottom contact

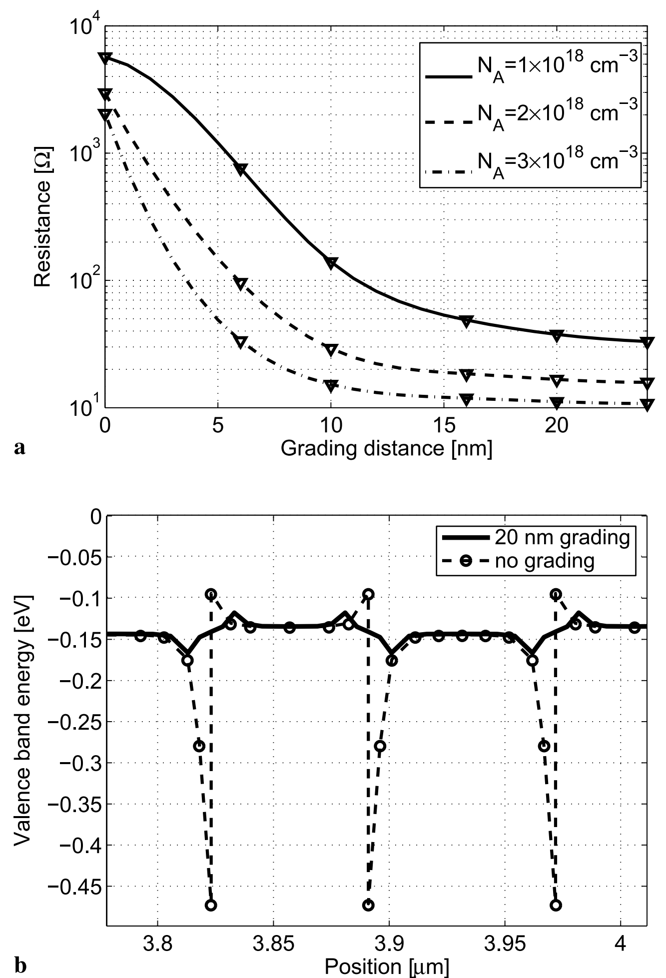

FIGURE 2 Influence of the grading distance on (**a**) the resistance of a p-type $Al_{0.9}Ga_{0.1}As/Al_{0.2}Ga_{0.8}As$ DBR with 10-µm radius and 30 periods for different acceptor concentrations N_A and (**b**) the valence-band edge at the interfaces

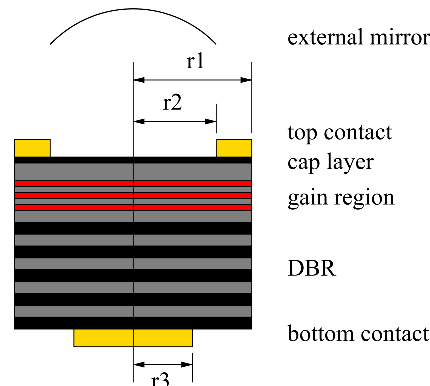

FIGURE 3 EP-VECSEL design with a ring top contact and a central disk bottom contact (not to scale)

radius r_3 is equal to the device radius r_1. However, this configuration yields spatial carrier distributions in the active region which are unsuitable for fundamental transverse mode operation with the field maximum in the center of the device. The n-DBR design, which provides a lower resistance and easier growth compared to the p-DBR structure, yields an increased charge-carrier concentration and thus inversion below

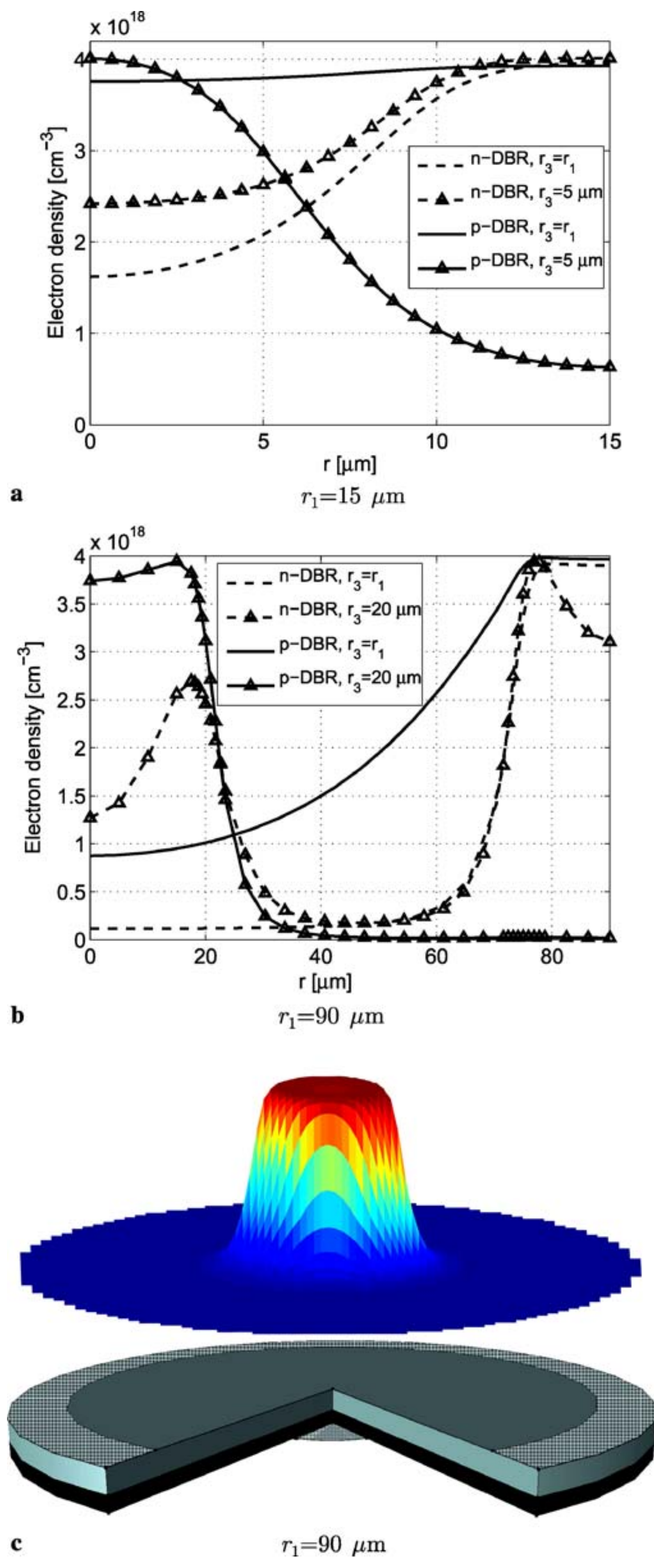

FIGURE 4 (**a**) and (**b**) Radial carrier distributions in the active gain region of an EP-VECSEL for different device radii and bottom contact designs. (**c**) Sketch of the sliced EP-VECSEL (true to scale) with p-DBR and $r_2 = 20\ \mu$m from (**b**) and the corresponding two-dimensional carrier density in the gain region. *Hatched areas* denote the top and bottom contacts

the top contact already for small device radii (see Fig. 4a). The p-mirror VECSEL allows for a flat spatial carrier distribution in small structures (cf. Fig. 4a), but also fails in confining the current for usual VECSEL device radii (see Fig. 4b). This contrast between p- and n-mirror design originates from the difference in electron and hole carrier mobilities. In order to enable current injection to the device center, the bottom contact could be implemented as a central disk contact with $r_3 < r_1$, which can be seen in Fig. 3. From an optical point of view the bottom contact is uncritical, because it is placed below the highly reflective DBR mirror where the laser field has strongly decayed. Nevertheless, simulations show that it plays a major role for the current confinement. If the bottom mirror is n-doped a central disk bottom contact slightly improves the radial carrier distributions in small devices, but the highest inversion is still obtained at the device boundary (cf. Fig. 4a). Figure 4b shows the injected carrier concentration in the active region of a broad VECSEL structure with peaks close to the contact edges. Hence, an n-DBR design is not suitable for TEM_{00} operation. Unlike the n-mirror structure, a p-DBR VECSEL with a disk contact allows for current confinement to the device center (see Fig. 4). This also holds true for large device radii, enabling power scaling even if the shape of the radial carrier distribution slightly deteriorates. Note that the results in Fig. 4 have been obtained with different applied biases due to the unequal resistances of the presented designs. The injected carrier concentration in the active region falls off very quickly for radial positions beyond the bottom contact radius r_3 in a p-DBR VECSEL (cf. Fig. 5a). It is observed that, due to the hole mobility being much smaller than the electron mobility, there is hardly any carrier spread in the lateral direction in the p-mirror and the electrons injected from the top ring contact follow the spatial hole distribution. Since the hole current is confined by the bottom disk contact size, the device resistance scales inversely with the bottom contact radius in EP-VECSELs featuring a bottom p-DBR (cf. Fig. 5b). This is advantageous for power scaling, which is obtained by increasing the lateral dimension of the device and the pumped region and thus by increasing the bottom contact size. In Fig. 5b it can further be seen that the device resistance is dominated by the hole current, since a change of the aperture radius r_2 keeping the bottom contact size yields only a minor resistance change. The influence of the bottom contact size on the device performance is much less in an n-doped bottom DBR design due to the high electron mobility, which leads to considerable current spreading in the mirror. Additionally, the holes injected via the ring top contact in a bottom n-DBR design spread much less than electrons before reaching the active QWs. Thus, uniform current injection into the active gain region cannot be achieved satisfactorily (cf. Fig. 4). This makes the design of an EP-VECSEL with an n-doped DBR unfeasible, at least, if no additional carrier-confining elements are introduced into the device. In contrast, fundamental mode operation could be achieved in a p-DBR EP-VECSEL with a central bottom contact. Aside from the advantages of a disk bottom contact mentioned above, processing is complicated, since a central alignment of the disk contact has to be ensured.

3.2 *Current-spreading layer or cap layer*

Figure 5a reveals that larger mode areas supported by larger bottom contact radii demand additional measures to confine the carriers to the device center and thus increase

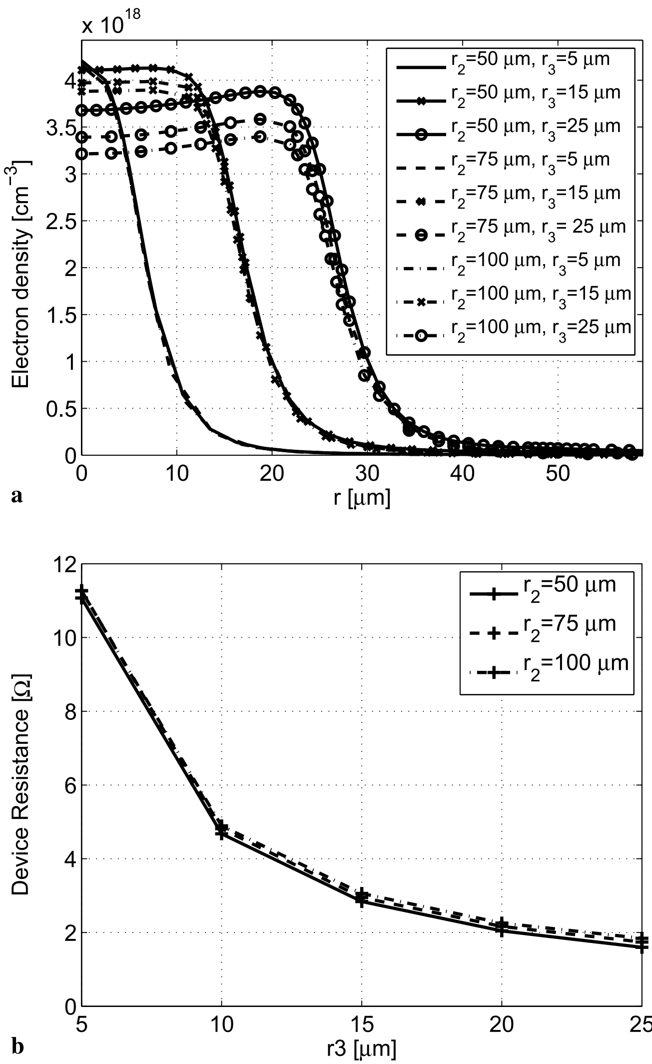

FIGURE 5 Influence of the bottom contact radius r_3 for a device with a bottom p-DBR and an aperture radius r_2 on (**a**) the carrier distribution along the radial axis in the active gain region and (**b**) the device resistance

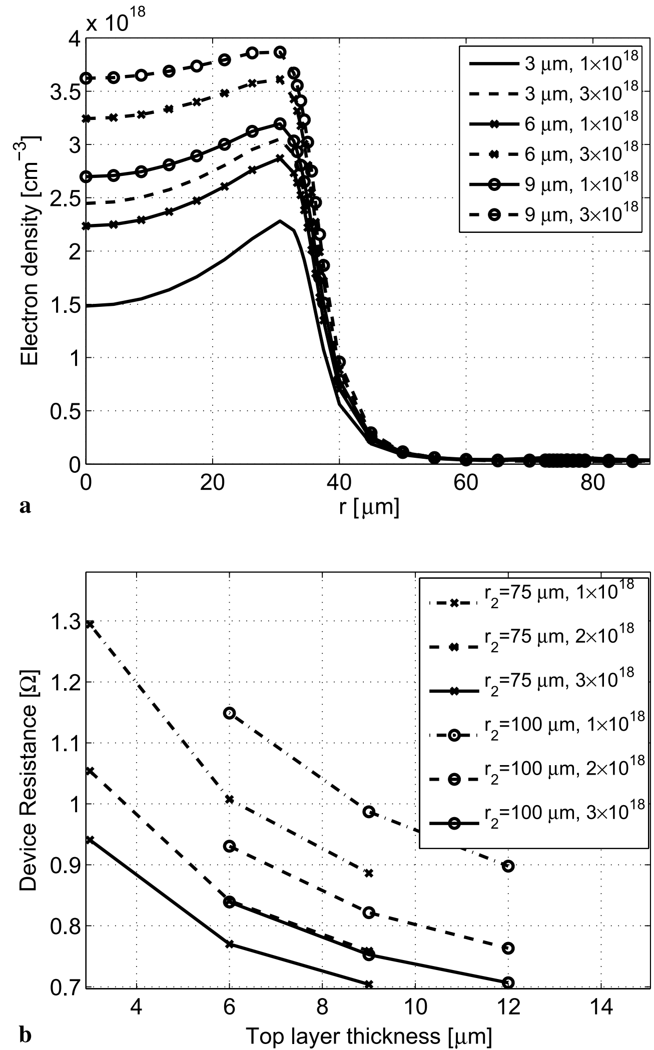

FIGURE 6 Influence of the top-layer thickness and doping (in cm^{-3}) on (**a**) the carrier distribution along the radial axis in the active gain region ($r_2 = 75\,\mu m$) and (**b**) the device resistance for a device with a bottom p-DBR with 35-μm radius

the fundamental transverse mode gain. Simulations show that the aspect ratio of the top electron injection layer is too large, such that the electrons cannot reach the device center. Hence, a high-mobility cap or current-spreading layer is introduced below the top ring contact. Contacting a device while at the same time allowing for out- or in-coupling of light is quite a common problem in opto-electronic devices and a variety of cap-layer designs has been proposed. One possibility is the use of wide band gap oxide semiconductors like indium tin oxide (ITO) or zinc oxide (ZnO), which are widespread in the solar-cell market and have been applied to edge emitters and VCSELs [26, 27]. Another solution are highly doped GaAs layers. A low resistivity of the cap layer is desired to decrease overall device resistance (Joule heating) and enabling current confinement to the center of the device for maximum TEM_{00} gain. This has to be combined with a low optical absorption to minimize the losses and a low contact resistance to the metal contact. Highly doped ITO films with doping concentrations as large as $2 \times 10^{21}\,cm^{-3}$ yield resistivities down to $1 \times 10^{-4}\,\Omega\,cm$ [28]. ZnO films, which have been investigated more recently, are interesting due to their potentially lower cost compared to ITO. Their resistivity values reach from $1 \times 10^{-3}\,\Omega\,cm$ at a doping level of $4 \times 10^{20}\,cm^{-3}$ [29] to $2 \times 10^{-4}\,\Omega\,cm$ for doping concentrations above $10^{21}\,cm^{-3}$ [30]. With highly doped GaAs layers comparable resistivities can already be obtained with much lower doping. N-doped GaAs with $N_D = 1 \times 10^{19}\,cm^{-3}$, for example, exhibits $\varrho \approx 4 \times 10^{-4}\,\Omega\,cm$ [31, 32], which is in the range of $1 \times 10^{21}\,cm^{-3}$-doped n-ZnO [30]. The FCA absorption coefficient of doped GaAs is known to be $\alpha = 5 \times 10^{-18}\,cm^2 \cdot n + 11 \times 10^{-18}\,cm^2 \cdot p$, where n and p denote the electron and hole densities, respectively. Using a plane-wave approach and neglecting standing wave effects the optical loss can be approximated by $\exp(\alpha/2d)$, with d being the thickness of the cap layer. This yields a loss well below 1% for a highly doped 200-nm-thick current-spreading layer. This value can be further decreased if the layer resides in a standing wave node. Unlike GaAs, ITO and ZnO are transparent over the complete visual range, but exhibit rather high FCA losses of several percent for the same layer thickness in the near-infrared region where InGaAs/AlGaAs VECSELs are oper-

ated [27, 29]. This is due to the very high doping levels and low carrier mobilities in these materials. Other transparent conductive oxides might be available in the future, yielding lower FCA than highly doped GaAs at comparable resistivities [33]. However, in the design study presented, a GaAs cap layer is chosen due to the low loss and to simplify the growth of the structure. This allows in the same run the growth of an AR coating on top of the conducting layer to reduce the dispersion and improve mode-locking operation.

To exploit the power scalability of disk lasers, p-mirror VECSELs with an aperture radius r_2 of up to 100 μm and large bottom contact radii should be feasible. In such devices a thin highly doped cap layer as applied in VCSELs [17] is not sufficient to obtain uniform current injection at the device center. However, the uniformity of the injected charge-carrier distribution above the bottom contact can be enhanced by increasing the cap-layer thickness or doping concentration, as can be seen in Fig. 6a. The larger doping concentration leads to a decrease of the resistivity of the top layer, yielding a lower overall device resistance and a smaller resistance to current flow from the ring contact to the center of the device. The increased layer thickness has a similar effect, since it reduces the sheet resistance to radial current flow and thus the device resistance (cf. Fig. 6b). The result is the above-mentioned greater uniformity of the pumped carrier concentrations in the active region. However, an increased thickness as well as higher doping of the top layer increase the optical loss due to FCA. The additional round trip FCA loss introduced by an n-doped top layer can be given as $\exp(-5\times10^{-18}\,\text{cm}^2\cdot n\cdot d)$, with n denoting the carrier concentration that approximately equals the doping concentration and d being the layer thickness. Hence, equal $d\times N_{\text{D}}$ values yield approximately the same optical loss. The simulation results in Fig. 6a show that, for greater thickness and lower doping at a fixed $d\times N_{\text{D}}$ value, a more uniform radial carrier distribution is obtained. Moreover, a larger back-contact radius for a broader mode and higher output power demands a greater top-layer thickness, which can be seen on comparing Figs. 6a and 7. Thus, a moderately doped thick GaAs cap layer is combined with a thin highly doped GaAs cap layer, which allows for satisfactory contacting of the device. The highly doped layer should be placed into a standing wave node to minimize optical losses. However, the alignment is hindered by the large layer thickness underneath. In a p-mirror design the thick current-spreading layer within the cavity is n-doped with approximately half the FCA compared to a p-doped layer. Furthermore, the optical intensity decreases very fast in the p-mirror. Thus, a p-mirror design is also superior to an n-DBR VECSEL in terms of optical losses. Cap layers comprising hitherto available transparent conducting oxides like ITO or ZnO are also detrimental to the device performance. This is due to their higher optical loss at the operation wavelength compared to GaAs layers with the same resistivity. For the choice of the cap-layer thickness and doping a trade off between device resistance and current confinement on the one hand and optical loss on the other hand has to be found.

3.3 *Tunnel junctions and oxides*

The simulation results in the preceding sections showed that an n-DBR VECSEL cannot be satisfactorily pumped electrically without additional carrier-confining elements. Such structures, like tunnel junctions [34] or oxide barriers [35], which have been applied in VCSEL design, could also be integrated between the active region and the top ring contact of a VECSEL. However, an oxide barrier influences the optical mode and, therefore, has to be located at the node of the standing wave to minimize this effect. Furthermore, the oxidation makes the device processing more difficult. Another disadvantage of the oxide barrier is current crowding occurring at the oxide-barrier tip, which leads to a strongly nonuniform spatial carrier distribution in the active region (cf. Fig. 8) for devices with large lateral dimensions and an n-type bottom mirror. Hence, this design is not suitable for maximizing the fundamental transverse mode gain in VECSELs. A structured tunnel junction for current

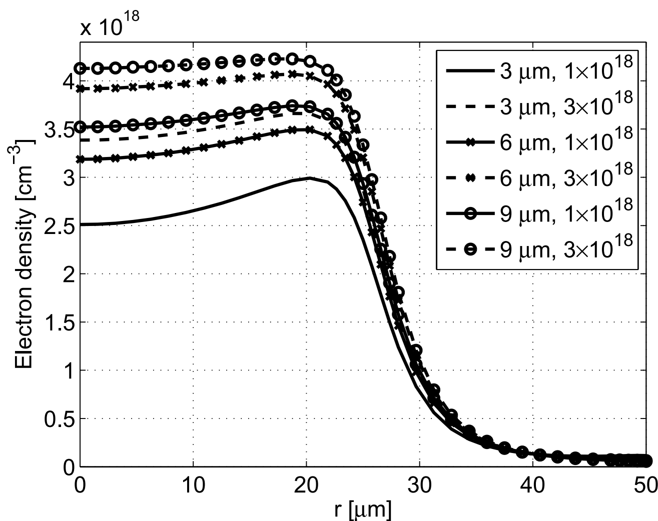

FIGURE 7 Carrier distribution along the radial axis in the active region. The device exhibits a bottom contact radius $r_3 = 25$ μm, an aperture radius $r_2 = 50$ μm, and a bottom p-DBR. Doping is given in cm^{-3}

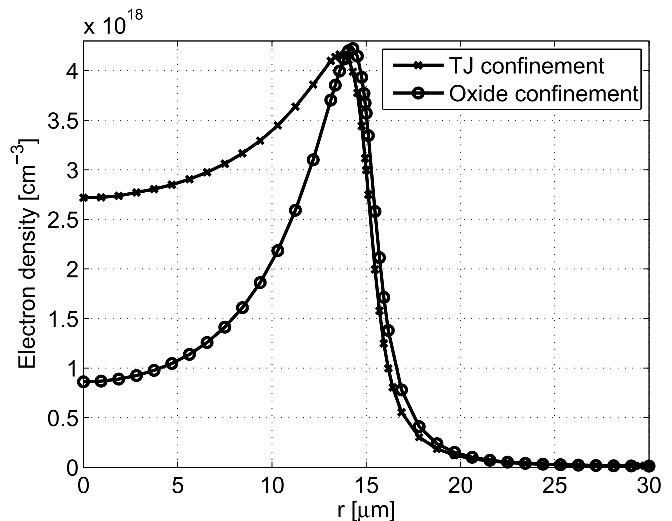

FIGURE 8 Carrier distribution along the radial axis in the active region. The device exhibits a current confinement structure with 15-μm aperture, $r_2 = 30$ μm, and a bottom n-DBR

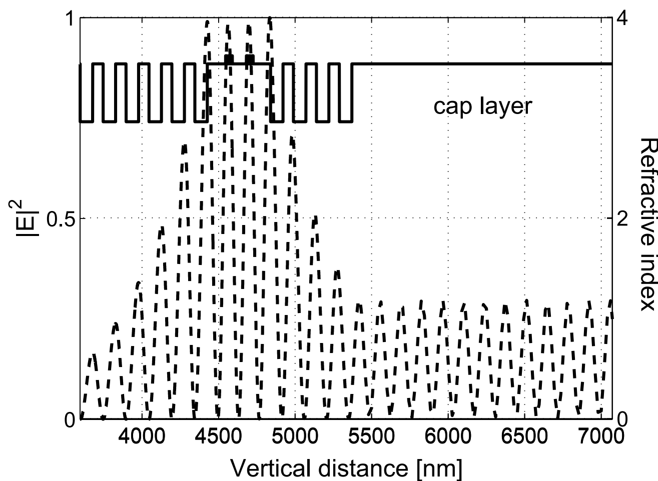

FIGURE 9 Refractive index and field profile of the active region with a low-reflective top DBR for confinement-factor enhancement

confinement demands sophisticated growth and processing. Furthermore, it introduces additional FCA loss due to the high doping concentrations ($\sim 1 \times 10^{20}$ cm^{-3}). This prohibits laser operation if the tunnel junction is not placed in the node of the standing wave. While this approach, like an oxide barrier, works well for device radii as found in VCSELs, it does not yield a satisfactory spatial carrier distribution in the gain QWs (see Fig. 8) of an n-DBR VECSEL. The difference between the tunnel junction and oxide confinement is due to the fact that, in the case of the oxide confinement, holes with a low mobility are injected from the top contact. In contrast, in a tunnel junction design, electrons with higher mobility are injected from the ring contact. Comparing the results for these designs with the p-DBR design with central bottom contact (cf. Fig. 7) illustrates the superior carrier-confinement capabilities of the latter, which allow for scaling of the mode area to obtain high output powers. This is not possible with an n-DBR design, even if a tunnel junction or oxide barrier is included. In p-DBR devices with a central disk bottom contact and oxide barriers or structured tunnel junctions below the top contact, simulations yield a radial QW carrier distribution comparable to the same device without these additional confining structures. In addition to the top contact and cap-layer designs above there are also approaches with thin metal current-spreading layers [36], which have been demonstrated in VCSELs. However, the alignment of such layers is very critical to avoid prohibitive optical losses and simulations showed no satisfactory current injection for the large device radii of VECSELs.

3.4 *Gain region*

The optical losses in an EP-VECSEL structure with a thick n-doped top layer for current spreading are rather high. These losses have to be compensated by an active region with sufficient modal gain. To achieve maximum mode gain, the active QWs have to reside in standing wave antinodes, which corresponds to a high enhancement factor for the electric field distribution [37]. Usually, several QWs are placed into one antinode, but their number is limited by the width of the standing wave peak. If higher gain is desired, two groups of QWs can be arranged in adjacent field maxima. Another possibility is the increase of the enhancement factor by introducing a low-reflective DBR between the active gain region and the cap layer (see Fig. 9), which also reduces the cavity losses by decreasing the field strength in the doped top layer. However, the sub-cavity between the two DBRs has a strong spectral filtering effect [3], which reduces the bandwidth of the device. Hence, the minimum achievable pulse width by mode locking is increased. Without an AR coating on top of the device, the thick cap layer would result in a second sub-cavity, further deteriorating device performance.

3.5 *Final design and mode locking*

Taking into account all of the above considerations, the EP-VECSEL structure depicted in Fig. 10 eventually emerges as the best suited for power scaling among the presented designs. Its optical loss, which is introduced mainly by the thick n-doped cap layer, must be compensated by a large mode gain. However, FCA losses are smaller than in designs with a p-doped current-spreading layer. The resistance of the device can be kept moderate by grading the heterointerfaces in the p-mirror. Furthermore, apart from the interface grading and bottom contact alignment the growth and processing is kept as easy as possible. Note that a design with a bottom n-DBR is not suitable for fundamental transverse mode operation in large-area laser structures due to the poor carrier confinement.

The presented design is suitable to be directly mode locked using an external SESAM as demonstrated in optically pumped VECSELs (OP-VECSELs) [4]. Quantum-dot SESAMS (QD-SESAMs) have been successfully developed for 1 : 1 mode locking, where the spot sizes on the VECSEL and the SESAM are equal [38]. This is required for the integration of the absorber into the VECSEL. Such integration has been recently demonstrated with the optically pumped MIXSEL (OP-MIXSEL) [10]. For stable mode-locking operation, the saturation energy of the absorber has to be lower than for the gain [4, 10]. The ratio can be controlled by the field enhancement and the intrinsic absorber properties [37]. In the OP-MIXSEL [10], the saturable absorber has a higher field enhancement and QDs have been used to lower the modulation depth by adjusting the quantum-dot density ac-

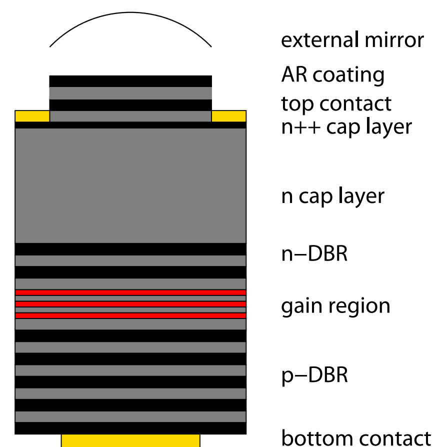

FIGURE 10 Sketch of the optimized EP-VECSEL design (not to scale)

cordingly. A single QD absorber layer was sufficient for stable passive mode locking.

The best current EP-VECSEL design as shown in Fig. 10 has the added advantage that it is compatible with an EP-MIXSEL design. The QD SESAM absorber would ideally be integrated in the unpumped AR coating section. This section can be designed to obtain the required field enhancement in the absorber and to couple the light out of the EP-MIXSEL with minimized reflections for good mode locking.

4 Conclusion

We have presented a systematic design optimization of EP-VECSELs backed by numerical simulations. A drift–diffusion model has been used for the carrier transport and a transfer-matrix method for optical loss simulation. Simulations show that a n-doped bottom mirror is not suited to provide fundamental transverse mode operation in a large-area VECSEL. Furthermore, the superiority of a structured bottom contact to tunnel junctions and oxide barriers for carrier confinement in the active region is pointed out. The p-DBR as well as the cap layer and active region have been investigated in detail and an optimized EP-VECSEL structure has been derived.

Future work will be devoted to coupled electro-optical simulations above threshold and electro-opto-thermal simulations including a thermodynamic model accounting for self heating of the device.

ACKNOWLEDGEMENTS This work was supported by ETH Zurich with research grant TH-46/05-2 E-VECSEL and by the Intel Corporation through a university sponsored research agreement.

OPEN ACCESS This article is distributed under the terms of the Creative Commons Attribution Noncommercial License which permits any noncommercial use, distribution, and reproduction in any medium, provided the original author(s) and source are credited.

REFERENCES

1 M. Kuznetsov, F. Hakimi, R. Sprague, A. Mooradian, IEEE Photon. Technol. Lett. **9**, 1063 (1997)
2 J. Chilla, S. Butterworth, A. Zeitschel, J. Charles, A. Caprara, M. Reed, L. Spinelli, Proc. SPIE **5332**, 143 (2004)
3 A.C. Tropper, H.D. Foreman, A. Garnache, K.G. Wilcox, S.H. Hoogland, J. Phys. D **37**, R75 (2004)
4 U. Keller, A.C. Tropper, Phys. Rep. **429**, 67 (2006)
5 U. Keller, K.J. Weingarten, F.X. Kartner, D. Kopf, B. Braun, I.D. Jung, R. Fluck, C. Honninger, N. Matuschek, J. Aus der Au, IEEE J. Sel. Top. Quantum Electron. **2**, 435 (1996)
6 S. Hoogland, S. Dhanjal, A.C. Tropper, J.S. Roberts, R. Häring, R. Paschotta, F. Morier-Genoud, U. Keller, IEEE Photon. Technol. Lett. **12**, 1135 (2000)
7 R. Häring, R. Paschotta, A. Aschwanden, E. Gini, F. Morier-Genoud, U. Keller, IEEE J. Quantum Electron. **QE-38**, 1268 (2002)
8 A. Aschwanden, D. Lorenser, H.J. Unold, R. Paschotta, Appl. Phys. Lett. **86**, 1102 (2005)
9 S. Hoogland, A. Garnache, I. Sagnes, J.S. Roberts, A.C. Tropper, IEEE Photon. Technol. Lett. **17**, 267 (2005)
10 D.J.H.C. Maas, A.-R. Bellancourt, B. Rudin, M. Golling, H.J. Unold, T. Südmeyer, U. Keller, Appl. Phys. B **88**, 493 (2007)
11 A. Bousseksou, M. El Kurdi, M.D. Salik, I. Sagnes, S. Bouchoule, Electron. Lett. **40**, 1490 (2004)
12 M. El Kurdi, S. Bouchoule, A. Bousseksou, I. Sagnes, A. Plais, M. Strassner, C. Symonds, A. Garnache, J. Jacquet, Electron. Lett. **40**, 671 (2004)
13 E.M. Strzelecka, J.G. McInerney, A. Mooradian, A. Lewis, A.V. Shchegrov, D. Lee, J.P. Watson, K.W. Kennedy, G.P. Carey, H. Zhou, W. Ha, B.D. Cantos, W.R. Hitchens, D.L. Heald, V.V. Doan, K.L. Lear, Proc. SPIE **4993**, 57 (2003)
14 Q. Zhang, K. Jasim, A.V. Nurmikko, A. Mooradian, G. Carey, W. Ha, E. Ippen, IEEE Photon. Technol. Lett. **16**, 885 (2004)
15 G.A. Keeler, D.K. Serkland, K.M. Geib, G.M. Peake, A. Mar, IEEE Photon. Technol. Lett. **17**, 522 (2005)
16 K. Jasim, Q. Zhang, A.V. Nurmikko, A. Mooradian, G. Carey, W. Ha, E. Ippen, Electron. Lett. **39**, 373 (2003)
17 C. Wilmsen, H. Temkin, L.A. Coldren (eds.), *Vertical-Cavity Surface-Emitting Lasers: Design, Fabrication, Characterization, and Applications* (Camb. Stud. Mod. Opt.) (Cambridge University Press, New York, 1999)
18 B. Witzigmann, A. Bäcker, S. Odermatt, J. Comput. Theor. Nanosci. (2007) invited contribution, to appear
19 S. Selberherr, *Analysis and Simulation of Semiconductor Devices* (Springer, New York, 1984)
20 B. Witzigmann, *Design and Implementation of a Three-Dimensional Edge Emitting Quantum Well Laser Simulator* (Ser. Microelectron. **102**) (Hartung-Gorre, Konstanz, 2000)
21 D. Schroeder, *Modelling of Interface Carrier Transport for Device Simulation, Computational Microelectronics* (Springer, Wien New York, 1994)
22 J. Mulet, S. Balle, IEEE J. Quantum Electron. **QE-41**, 1148 (2005)
23 M.G. Peters, B.J. Thibeault, D.B. Young, J.W. Scott, F.H. Peter, A.C. Gossard, L.A. Coldren, Appl. Phys. Lett. **63**, 3411 (1993)
24 D.W. Winston, R.E. Hayes, IEEE J. Quantum Electron. **QE-34**, 707 (1998)
25 S. Odermatt, *Physics and Simulation of Semiconductor Lasers: Static and Dynamic Characteristics* (Ser. Microelectron. **177**) (Hartung-Gorre, Konstanz, 2006)
26 X. Wang, B. Lu, S.D. Hersee, IEEE Photon. Technol. Lett. **8**, 49 (1996)
27 C.L. Chua, R.L. Thornton, D.W. Treat, V.K. Yang, C.C. Dunnrowicz, IEEE Photon. Technol. Lett. **9**, 551 (1997)
28 C.G. Granqvist, A. Hultåker, Thin Solid Films **411**, 1 (2002)
29 J. Steinhauser, L. Feitknecht, S. Fay, R. Schlüchter, J. Springer, A. Shah, C. Ballif, Effect of rough ZnO layers in improving performances of microcrystalline silicon solar cells, in *Proc. 20th Eur. Photovoltaic Solar Energy Conf.*, Barcelona, Spain, June 2005, pp. 1608–1611
30 K. Ellmer, J. Phys. D **34**, 3097 (2001)
31 S. Adachi (ed.), *Properties of Aluminium Gallium Arsenide* (INSPEC, London, 1993)
32 W.C. Liu, J. Mater. Sci. **25**, 1765 (1990)
33 T. Koida, M. Kondo, J. Appl. Phys. **101**, 063 705 (2007)
34 M. Ortsiefer, R. Shau, G. Böhm, F. Köhler, M.-C. Amann, Appl. Phys. Lett. **76**, 2179 (2000)
35 D.G. Deppe, D.L. Huffaker, J. Shin, Q. Deng, Photon. Technol. Lett. **7**, 965 (1995)
36 D.F. Feezell, R.M. Farrell, M.C. Schmidt, H. Yamada, M. Ishida, S.P. DenBaars, D.A. Cohen, S. Nakamura, Appl. Phys. Lett. **90**, 181 128-1 (2007)
37 G.J. Spühler, K.J. Weingarten, R. Grange, L. Krainer, M. Haiml, V. Liverini, M. Golling, S. Schön, U. Keller, Appl. Phys. B **81**, 27 (2005)
38 D. Lorenser, D.J.H.C. Maas, H.J. Unold, A.R. Bellancourt, B. Rudin, E. Gini, D. Ebling, U. Keller, IEEE J. Quantum Electron. **QE-42**, 838 (2006)